

Experimental scaling of fluctuations and confinement with Lundquist number in the reversed-field pinch

M. R. Stoneking,^{a)} J. T. Chapman, D. J. Den Hartog, S. C. Prager, and J. S. Sarff
Department of Physics, University of Wisconsin—Madison, Madison, Wisconsin 53706

(Received 18 September 1997; accepted 12 January 1998)

The scaling of the magnetic and velocity fluctuations with Lundquist number (S) is examined experimentally over a range of values from 7×10^4 to 10^6 in a reversed-field pinch (RFP) plasma. Magnetic fluctuations do not scale uniquely with the Lundquist number. At high (relative) density, fluctuations scale as $\tilde{b} \propto S^{-0.18}$, in agreement with recent numerical results. Fluctuations are almost independent of S at low (relative) density, $\tilde{b} \propto S^{-0.07}$. The range of measured exponents is narrow and is in clear disagreement with theories predicting $\tilde{b} \propto S^{-1/2}$. At high relative density, the scaling of the energy confinement time follows expectations for transport in a stochastic magnetic field. A confinement scaling law ($n\tau_E \propto \beta^{4/5} \cdot T^{-7/10} \cdot a^{-3/5} \cdot I_\phi^2$) is derived, assuming the persistent dominance of stochastic magnetic diffusion in the RFP and employing the measured scaling of magnetic fluctuations. The peak velocity fluctuations during a sawtooth cycle scale marginally stronger than magnetic fluctuations but weaker than a simple Ohm's law prediction. The sawtooth period is determined by a resistive-Alfvénic hybrid time ($T_{\text{saw}} \propto \sqrt{\tau_R \tau_A}$) rather than a purely resistive time. © 1998 American Institute of Physics. [S1070-664X(98)03304-7]

I. INTRODUCTION AND BACKGROUND

Resistive magnetohydrodynamics (MHD) successfully describes much of the dynamics of the reversed-field pinch (RFP). For example, the sustainment of a reversed toroidal magnetic field in the presence of a purely toroidal applied electric field is observed in MHD simulations to result from the nonlinear interaction of resistive tearing instabilities,¹⁻⁴ a phenomenon called the *RFP dynamo*. Magnetic fluctuations consistent with an interpretation of tearing modes are observed in experiments,⁵⁻⁷ and the dynamo electric field has been measured at the edge of the RFP.⁸ Experiments display global relaxation events, hereafter ‘‘sawteeth.’’⁹⁻¹¹ Sawteeth are also seen in MHD simulations,¹²⁻¹⁴ and the nonlinear coupling of the dominant tearing modes seen in the simulations is qualitatively consistent with measurements.¹⁵ Saturated fluctuation levels (normalized to the mean field) are ~ 2 times higher in simulations than in experiment, a small discrepancy generally ascribed to the fact that simulations are conducted at a lower Lundquist number than is realized in experiments. The Lundquist number, $S = \tau_R / \tau_A$, is the ratio of the resistive diffusion time, $\tau_R = \mu_0 a^2 / \eta$, to the Alfvén time, $\tau_A = a / v_A$, where η is the electrical resistivity and v_A is the Alfvén velocity. The importance of resistive dissipation on the time scale of MHD motions is determined by S . To accurately model plasmas with high S requires fine spatial resolution and therefore long computation times.

The equations for (pressureless) resistive MHD can be cast into a dimensionless form as

$$\frac{\partial \mathbf{B}}{\partial t} = \nabla \times (\mathbf{v} \times \mathbf{B}) + \frac{1}{S} \nabla^2 \mathbf{B}, \quad (1)$$

^{a)}Present address: Department of Physics, Lawrence University, Appleton, Wisconsin 54911.

$$\frac{\partial \mathbf{v}}{\partial t} + (\mathbf{v} \cdot \nabla) \mathbf{v} = (\nabla \times \mathbf{B}) \times \mathbf{B} + \frac{1}{R_e} \nabla^2 \mathbf{v}. \quad (2)$$

The magnetic field is normalized to a typical field value (equilibrium field). Velocity is normalized to the Alfvén velocity, $v_A = B / \sqrt{\rho \mu_0}$. Spatial coordinates are normalized to the plasma size, a , and time to the Alfvén time. The Reynolds-like number, R_e , is the ratio of the momentum diffusion time $\tau_{\text{momentum}} = a^2 / \nu$, to the Alfvén time, where ν is the viscosity. In MHD theory of the RFP, the Lundquist number is the relevant dimensionless parameter rather than R_e (or some other combination of resistivity and viscosity, such as the Hartmann number or the magnetic Prandtl number) because plasma kinetic energy is dominated by the magnetic energy ($\beta \sim 2 \mu_0 n T / B^2$ is small and the mean flow velocities are small compared to the Alfvén velocity). Said another way, resistive dissipation dominates viscous dissipation by orders of magnitude.

In this paper we report on measurements of the scaling of magnetic fluctuations, velocity fluctuations, and energy confinement in a RFP with variations in the Lundquist number. The experiments were motivated by a desire to resolve conflicting theoretical predictions (both numerical and analytic) for fluctuation scaling in the RFP, to extend scaling results from previous experiments to higher S using a more complete experimental determination of the resistivity than was used in previous experiments, and to permit more reliable extrapolation toward RFP reactor conditions.

A simple theoretical prediction for S scaling of fluctuations is found from the dimensionless Ohm's law,

$$S (E_{\parallel} + \langle \tilde{\mathbf{v}} \times \tilde{\mathbf{b}} \rangle_{\parallel}) = J_{\parallel}, \quad (3)$$

where $\tilde{b} \equiv \tilde{B} / B_0$, $\tilde{v} \equiv \tilde{v} / v_A$, the current density is normalized to $B_0 / \mu_0 a$, and the electric field is normalized to $v_A B_0$.

Assuming that the normalized magnetic and kinetic fluctuations scale with the same power of the Lundquist number yields a prediction that both the fluctuations should scale as $\tilde{b} = \tilde{v} \propto S^{-1/2}$ (see, for example, Ref. 16). The prediction is most easily seen by evaluating Eq. (3) at the toroidal field reversal radius, where $E_{\parallel} = 0$. This naive prediction neglects the possible scaling of the relative phase between \tilde{v} and \tilde{b} . Dimensional analysis of resistive MHD performed by Connor and Taylor¹⁷ also implies a scaling of $\tilde{b} \propto S^{-1/2}$. An *et al.*¹⁸ performed a turbulence theory calculation to obtain $\tilde{b} \propto S^{-1/3}$, but Matorr¹⁹ finds by a similar method that the scaling can be $\tilde{b} \propto S^{-1/4}$ or $\tilde{b} \propto S^0$ depending on the continuous or discrete nature of the RFP dynamo fluctuations, respectively (see Ref. 19 for a more complete review and critique of analytic predictions for Lundquist number scaling of fluctuations in the RFP). The experimental results presented in this paper contribute to a determination of the correct theoretical description. In particular, the theories predicting $\tilde{b} \propto S^{-1/2}$ are at odds with experimental results in the Madison Symmetric Torus (MST).

The first MHD computation that tested the Lundquist number scaling of magnetic fluctuations in the RFP was done by Strauss, who obtained $b \propto S^{-0.31}$ using a set of reduced MHD equations and covering a range of S values from 10^2 to 2×10^3 .²⁰ More recent works that go to a higher Lundquist number and use the complete three-dimensional (3-D) MHD equations have found fluctuation amplitudes to scale as $S^{-0.22}$ ($1.1 \times 10^3 < S < 10^5$)¹⁴ and $S^{-0.18}$ ($2.5 \times 10^3 < S < 4 \times 10^4$).²¹

On the experimental side, La Haye *et al.*⁶ measured the Lundquist number scaling of magnetic fluctuations in the OHTE device (operated as a RFP) and found $\tilde{b} \propto S^{-0.51}$. The Lundquist number was determined in OHTE by using the global plasma resistance and inductance to obtain a resistive diffusion time from $\tau_R = L/R$. The scaling thus obtained may be affected by anomalous resistance scaling as well as pure MHD effects. Hattori *et al.*²² inferred a Lundquist number scaling exponent (in TPE-1RM15) of approximately $-1/3$ for \tilde{b} by assuming that the Lundquist number scaled as the square of the plasma current. In the experiments reported in this paper we extend the measurement of fluctuation scaling in the RFP to a higher Lundquist number and obtain measurements of the Lundquist number by direct application of the Spitzer resistivity formula.

Recently, magnetic fluctuations associated with MHD turbulence (resistive tearing modes) have been apprehended as the principal cause of anomalous particle²³ and energy²⁴ transport in the core of the RFP. As fusion reactor plasmas will exist at a much higher Lundquist number than present experiments, a knowledge of the scaling of fluctuations in present experiments may provide useful predictions of transport rates in a RFP reactor. In addition, the results of these experiments may have implications for confinement in the spheromak, another low-field, relaxed state device with large-amplitude magnetic fluctuations.

In this work we report on the results of a Lundquist number scaling experiment in a RFP plasma. Scaling of confinement, magnetic fluctuations, velocity fluctuations, and

sawtooth features were probed over a range of S from 7×10^4 to 10^6 , S values significantly higher than those obtained in previous scaling studies in the RFP. In Sec. II, the experimental strategy and the coverage of parameter space are described. The method of determining the Lundquist number from measured quantities is also explained, and careful attention is paid to determining the scaling of the classical resistivity. Measurement of the classical resistivity and its use in determining S distinguish this work from past measurements of fluctuation scaling in the RFP.⁶ In MHD theory the Lundquist number is determined from the microscopic dissipation, as opposed to the additional MHD effects that contribute to experimental (global) resistance. Using the classical resistivity, therefore, provides a better comparison with theory than using the global resistance. The measurements that determine the Lundquist number are presented in Sec. III along with the values of S achieved. Bremsstrahlung measurements indicate the presence of significant impurity contamination ($Z_{\text{eff}} \sim 10$) at low current and low density, resulting in enhanced resistivity and a low Lundquist number in that parameter regime. Results of the scaling of magnetic fluctuations are presented in Sec. IV. We find that the global Lundquist number does not uniquely determine the fluctuation amplitude. At high (relative) density $\tilde{b} \propto S^{-0.18}$ and are almost independent of S at low (relative) density, $\tilde{b} \propto S^{-0.07}$. The observed variation in the scaling exponent may indicate the importance of an unidentified dimensionless parameter, or may be the result of profile variation not resolved by the global measurements used to obtain S . The range of exponents ($0.07 < \alpha < 0.18$) determined experimentally is quite narrow and falls in a range predicted by several of the theories reviewed above, and at high density agrees with recent 3-D MHD simulations. However, the results are incompatible with theories predicting $\tilde{b} \propto S^{-1/2}$, a scaling that has been used to plan the RFP program and guide it toward an attractive reactor design. The scaling of the energy confinement time (Sec. V) follows expectations for transport in a stochastic magnetic field, leading to a pessimistic confinement scaling law for an Ohmic RFP. The results suggest that a RFP reactor will require current profile control or some other fluctuation suppression measure to achieve the necessary transport levels for breakeven. Velocity fluctuation scaling is measured for the first time in a fusion relevant plasma experiment. The peak velocity fluctuation amplitude during the sawtooth cycle (presented in Sec. VI) scales marginally stronger than magnetic fluctuations but weaker than a simple Ohm's law prediction. The sawtooth period is governed by a resistive-Alfvénic hybrid time rather than a purely resistive time. Conclusions and a discussion of the main results are given in Sec. VII.

II. METHOD AND DEFINITIONS

A. Experimental method and parameter space coverage

The experiments reported here were conducted in the Madison Symmetric Torus (MST),²⁵ a reversed-field pinch with major radius of $R_0 = 1.5$ m and minor radius of $a = 0.52$ m. There are three principal control knobs for opera-

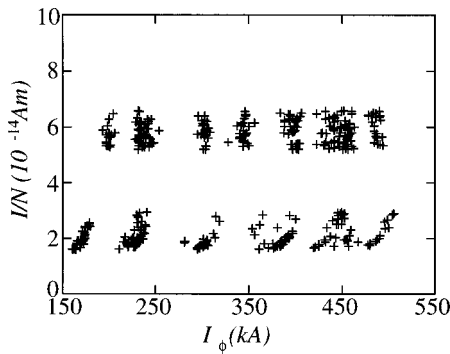


FIG. 1. The coverage of parameter space for the S -scaling experiment. Each point represents a 5 ms average during a single discharge. There are more than 300 discharges in the database. Shots were selected for two trajectories at constant I_ϕ/N .

tion of an Ohmic RFP: (1) the toroidal plasma current; (2) the plasma density; and (3) the toroidal flux. Alternately, the third control knob can be chosen as the ratio of the surface poloidal field to the volume-averaged toroidal field, the RFP pinch parameter Θ . The pinch parameter affects the field profiles [e.g., the plasma inductance in Eq. (9) below], but it has the weakest effect on the dependent variables (e.g., temperature, Lundquist number, confinement time, etc.), and therefore was held fixed for the experiments reported here. Maintaining a fixed pinch parameter was also motivated by a desire to fix the current profile shape, and thus maintain a similar free energy source for the dominant instabilities. Figure 1 is a summary of the parameter space coverage used for the S scaling experiment. Each point represents a 5 ms time average for a single discharge (the typical discharge duration is 60 ms with an ~ 15 ms flat top). The abscissa in Fig. 1 is the toroidal plasma current and the ordinate is the ratio of the toroidal plasma current to the line density through a central chord ($N = \bar{n} \pi a^2$). The full range of I_ϕ/N is obtainable at any plasma current (i.e., the parameter space I_ϕ/N vs I_ϕ is rectangular), whereas the experimentally obtainable density range depends on the plasma current. Shots were selected for two ranges of I_ϕ/N (> 150 shots in each set). The S scaling was examined separately for the two parameter space trajectories shown. The current scan at low I_ϕ/N is of particular interest for RFP reactor projections, as RFP experiments achieve the highest confinement for a particular plasma current near the highest density (lowest I_ϕ/N). The RFP density limit is a soft limit above which impurity and H_α/D_α radiation losses represent a significant fraction of the power supplied to the plasma, leading to confinement degradation and premature discharge termination.²⁶

B. Experimental definition of Lundquist number

A general definition of the Lundquist number can be expressed as

$$S = \frac{\tau_R}{\tau_A} = \frac{\mu_0 a^2}{\eta} \cdot \frac{B}{a \sqrt{\mu_0 m_i \bar{n}}}, \quad (4)$$

where the plasma minor radius, a , is taken as the appropriate scale length for the resistive diffusion time and the Alfvén

time. Although several of the quantities in Eq. (4) vary with radial position in the plasma, it is desirable to define a global Lundquist number by taking characteristic values for the magnetic field, density and resistivity. We use the surface poloidal magnetic field $B = \mu_0 I_\phi / 2\pi a$ and the central chord-averaged electron density, \bar{n} . The method of determining a characteristic resistivity is discussed next.

The resistivity can be expressed as^{27,28}

$$\begin{aligned} \eta_{\text{Spitzer}} &= \frac{m \langle v_{ei} \rangle^{Z=1}}{n_e e^2} \cdot \frac{3\pi}{32} \cdot \frac{Z_{\text{eff}}}{\gamma_E(Z_{\text{eff}})} \\ &= 5.22 \times 10^{-5} \frac{Z_\sigma \cdot \ln \Lambda}{T(\text{eV})^{3/2}} \Omega\text{m}, \end{aligned} \quad (5)$$

where $Z_{\text{eff}} = \sum n_i Z_i^2 / n_e$ is the mean ion charge and Z_σ is a function of Z_{eff} , following the notation of Hutchinson.²⁸ The first two factors on the left side constitute the Lorentz gas solution to the Fokker–Planck equation (electron–ion collisions only), and the last factor provides a correction that takes electron–electron collisions and multiple ion species into account (using the notation of Ref. 27). The functional relationship between Z_σ and Z_{eff} is taken from Hirshman and Sigmar,²⁹

$$\begin{aligned} Z_\sigma &= \frac{32}{3\pi} \cdot \gamma_E(Z_{\text{eff}} = 1) \cdot \frac{Z_{\text{eff}}(1 + 1.198Z_{\text{eff}} + 0.222Z_{\text{eff}}^2)}{(1 + 2.966Z_{\text{eff}} + 0.753Z_{\text{eff}}^2)} \\ &\approx 0.4 + 0.6Z_{\text{eff}}. \end{aligned} \quad (6)$$

The last expression is an approximate linearization that is convenient and sufficiently accurate for the range of Z_{eff} encountered in experiment. It should be noted that Z_σ is not directly proportional to Z_{eff} . Uncertainties in measurement of the absolute Z_{eff} therefore generate uncertainties in the scaling of the resistivity (and therefore the Lundquist number) with control parameters.

A complete determination of the classical resistivity in a toroidal device must take into account the presence of a trapped particle fraction. In the collisionless (or banana) regime where the collision frequency is less than the bounce frequency of the trapped particles, the trapped particle population enhances the Spitzer resistivity by a factor of order $1/(1-f_t)$, where f_t is the fraction of electrons that are trapped. For the experiments reported here the electron bounce frequency is more than five times the collision frequency (Fig. 17). The trapped particle fraction was determined from equilibrium modeling (details are given in the Appendix), and found to be $f_t \approx 0.38$. Because the RFP pinch parameter, Θ , was held fixed, the field profiles and therefore the trapped fraction do not vary with changes in the other control parameters, \bar{n} and I_ϕ .

Using Eqs. (4)–(6), we define an experimentally accessible global Lundquist number as

$$S_{\text{Spitzer}} = \frac{30 \cdot I_\phi T_{e0}^{3/2} (1-f_t)}{(0.4 + 0.6Z_{\text{eff}}) \ln \Lambda \sqrt{\mu_i \bar{n}}}, \quad (7)$$

where the toroidal plasma current, I_ϕ , is in kA, T_{e0} is the central electron temperature (in eV), \bar{n} is the central chord-averaged electron density (in units of 10^{19} m^{-3}), μ_i is the ion

mass (in amu), and $\ln \Lambda$ is the Coulomb logarithm. We label Eq. (7) the Spitzer Lundquist number, since it is defined by direct application of Spitzer's parallel resistivity formula. Deuterium was the working gas ($\mu_i=2$). Toroidal plasma current is measured by integrating the signal from a Rogowski coil that encircles the plasma column. Central electron temperature is measured with a single point, single pulse Thomson scattering system. A central interferometer chord provides a density measurement. Variations in the Coulomb logarithm were included in the scaling calculations shown below.

The mean ion charge was determined by measuring relative changes in the bremsstrahlung radiated power. Bremsstrahlung radiation was measured in two spectral bands: (1) the near infrared (1040 nm) and (2) the visible (532.5 nm). Both regions have been surveyed for and found to be free of spectral lines. Relative changes in the power detected in each band track each other, giving us additional confidence that spectral lines do not dominate either signal. In what follows, the visible bremsstrahlung detector signal was employed to determine relative Z_{eff} . In a narrow wavelength band (and over the fairly narrow temperature range obtained in the experiment) the bremsstrahlung radiation power depends on density, temperature, and ion charge as follows:

$$P_b \propto \frac{n_e^2 Z_{\text{eff}}}{T_e^{1/2}}. \quad (8)$$

Separate measurements of changes in bremsstrahlung power, density, and temperature therefore provide a measurement of relative changes in Z_{eff} .

In the OHTE experiment, not all of the quantities in Eq. (7) could be measured with the existing diagnostic set.⁶ La-Haye *et al.*, therefore, defined a Lundquist number in terms of the global plasma resistance,

$$S_{\text{anomalous}} = \frac{v_A}{a} \cdot \frac{L}{R}, \quad (9)$$

where L is the plasma inductance and R is the global plasma resistance ($R = V_\phi / I_\phi$, evaluated during the current flat top). We calculate both the Spitzer Lundquist number and the anomalous Lundquist number scaling of the magnetic fluctuations below. Numerically, the anomalous Lundquist number is significantly smaller than the Spitzer value for two reasons. First, the global resistance of the RFP is enhanced ($\sim 4X$) by the helical field trajectories ($B_\theta \approx B_\phi$), i.e., the so-called "screw-up factor." Second, RFPs are observed to have anomalously high resistivity (several times Spitzer).³⁰⁻³² We designate the value of S calculated from Eq. (9) anomalous because of its sensitivity to the anomalous resistivity.

The plasma inductance ($L \sim 2.6 \mu\text{H}$) used in Eq. (9) was estimated using the polynomial function model.³³ It is a constant for this experiment as the RFP pinch parameter was held fixed at $\Theta = 1.75 \pm 0.1$.

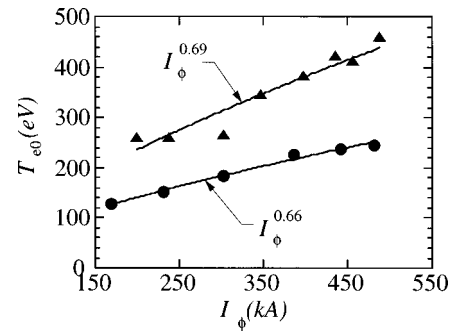


FIG. 2. The scaling of the central electron temperature with plasma current for low I_ϕ/N (circles) and high I_ϕ/N (triangles).

III. DETERMINATION OF LUNDQUIST NUMBER

A. Scaling of electron temperature with control parameters

Central electron temperature was measured with a single pulse, single point (central) Thomson scattering system.³⁴ Due to poor single shot statistics in the measured Thomson scattered spectrum, the spectra from a number of discharges with similar global parameters (I_ϕ and I_ϕ/N) were accumulated before determining the temperature. The current scaling of electron temperature was then determined for each of the fixed I_ϕ/N parameter space trajectories shown in Fig. 1. Figure 2 shows the temperature versus plasma current for the two I_ϕ/N values. The scaling obtained agrees qualitatively with previous temperature scaling measurements in MST.³⁵

B. Scaling of mean ion charge and resistivity with control parameters

A relative Z_{eff} is calculated from the detected bremsstrahlung power by normalizing out variations in temperature and density [see Eq. (8)]. An absolute Z_{eff} is assigned by scaling the relative Z_{eff} such that the lowest value obtained in the entire database is $Z_{\text{eff}}=1.0$. This normalization provides a lower bound on the true value of Z_{eff} . Figure 3 shows the variation in the mean ion charge for both current scans, as determined by the method just described. The lowest Z_{eff} is obtained at the highest absolute density (high plasma current, low I_ϕ/N). At the lowest absolute density Z_{eff} can exceed ~ 10 . Since all shots at a given plasma current and I_ϕ/N value were normalized with the same temperature value (as described above), Fig. 3 should be used to indicate the shot-averaged trend in Z_{eff} with changes in plasma current. For the purposes of scaling studies the trend is significant, as opposed to the value of Z_{eff} for individual shots.

Barring the possibility that unidentified line radiation is contaminating both bremsstrahlung spectral bands, this measurement indicates substantial aluminum contamination at low density in MST. The MST vacuum chamber is constructed of aluminum and is exposed to the plasma. Helium-like aluminum ($Z=11$) is the only impurity species in MST that could generate Z_{eff} values as high as 10. The normalized Z_{eff} (shot-averaged) values shown in Fig. 3 span the range from 1.0, an absolute lower bound, to ~ 11 , a reasonable upper bound for the known impurity species. The scaling of

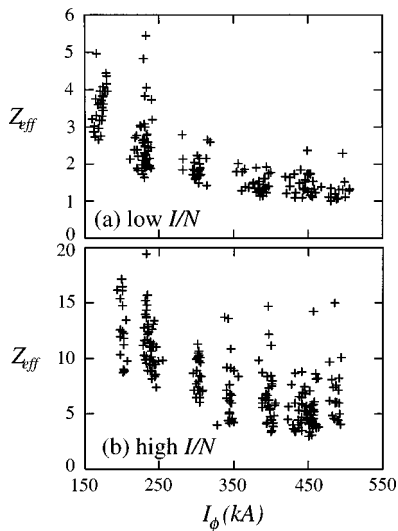


FIG. 3. We see Z_{eff} versus the plasma current for (a) low I_{ϕ}/N and (b) high I_{ϕ}/N . A visible bremsstrahlung signal was employed to get relative Z_{eff} . Signals were then scaled such that the minimum value of Z_{eff} in the database was 1.0.

relative Z_{eff} obtained from Fig. 3 therefore provides the true Z_{eff} scaling accurate to $\sim 25\%$ (e.g., $\langle Z_{\text{eff}} \rangle \approx 12 \pm 3$ at low-current, high I_{ϕ}/N).

A rough global comparison can be made between the experimental plasma resistance $R_{\text{exp}} = V_{\phi}/I_{\phi}$, and the Spitzer resistance, $R_{\text{Spitzer}} = 2R_0 g_{\text{RFP}} \eta_{\text{Spitzer}}/a^2(1-f_i)$, by assuming a flat resistivity profile. The screw-up factor, g_{RFP} , depends on the magnetic field profiles; $g_{\text{RFP}} = 4$ is used here.³³ The trapped particle fraction was $f_i \approx 0.38$. The ratio of the experimental resistance to the classical resistance is shown in Fig. 4. Measurement of the resistivity profile would likely resolve the apparently unphysical result that the global resistance is less than classical at high I_{ϕ}/N and low current. The global comparison makes use of a nominally central resistivity value and the resistivity profile is probably hollow. The

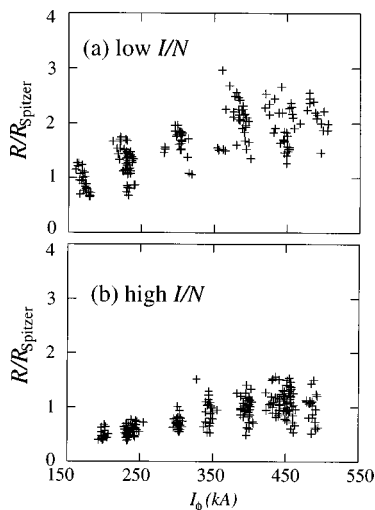


FIG. 4. A comparison of the global plasma resistance to the expected Spitzer value after resolving the dependence on the ion charge.

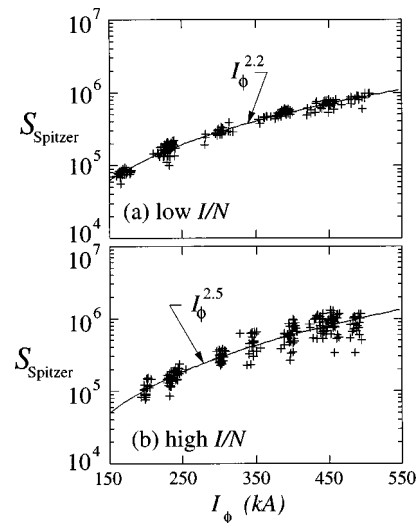


FIG. 5. Experimental determination of the Lundquist number at (a) low I_{ϕ}/N and (b) high I_{ϕ}/N .

comparison shown in Fig. 4 indicates that the resistivity anomaly in MST is largest at high current and high density (low I_{ϕ}/N).

C. Lundquist number

The experimentally determined Lundquist number calculated using Eq. (7) is shown in Fig. 5 for (a) low I_{ϕ}/N and (b) high I_{ϕ}/N . A range of about one decade in S was achieved for each scan. The variation in S at fixed plasma current is less than one decade, motivating the analysis of S scaling at fixed I_{ϕ}/N rather than fixed current. Although temperature drops with increasing density at a fixed current, the decrease in Z_{eff} at higher density keeps S from changing significantly. The Lundquist number scales somewhat stronger than the square of the plasma current and is roughly independent of density. Hattori *et al.* assumed that S scaled as the square of the plasma current in TPE-1RM15.²² That assumption was based on previous temperature and density scaling measurements in the same device, but did not resolve changes in Z_{eff} . Calculating the current scaling of S for MST data in the manner of Hattori *et al.*, we obtain $S \propto I_{\phi}^{1.5}$, due to weaker temperature scaling in MST, $T \propto I_{\phi}^{2/3}$ compared to $T \propto I_{\phi}$ in TPE-1RM15.

IV. SCALING OF AVERAGE MAGNETIC FLUCTUATION AMPLITUDE

The dominant fluctuations in the RFP are saturated, internally resonant resistive tearing modes. In MST, the tearing modes propagate presumably due to $\mathbf{E}_r \times \mathbf{B}$ and diamagnetic drifts giving them Doppler shifted frequencies in the range 10–20 kHz. Fluctuation measurements are made with an array of 32 toroidally separated *poloidal* field pickup coils attached to the inside of the vacuum vessel wall and spanning the entire toroidal circumference. Toroidal mode numbers $n \leq 15$ are resolved. The total fluctuation amplitude $\tilde{b}_n = \sqrt{\tilde{b}_{\theta,n}^2 + \tilde{b}_{\phi,n}^2}$ at the plasma surface in each mode, n , is obtained using the curl-free condition, $\mathbf{k} \times \tilde{\mathbf{b}} = 0$ and past

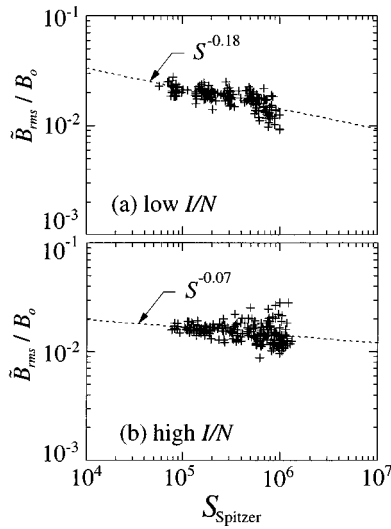
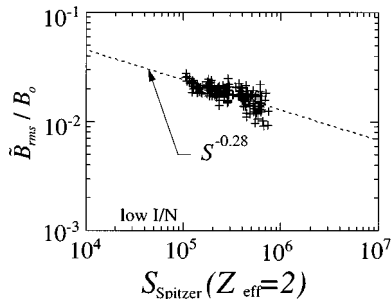
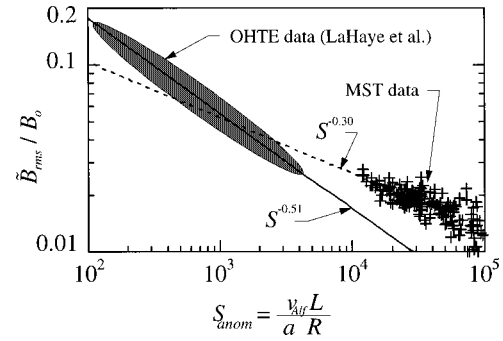


FIG. 6. The Lundquist number scaling of the rms magnetic fluctuations.

measurements of the polarization of each mode. The radial component is negligible since the plasma is bounded by a close-fitting conducting shell. The dominant modes (toroidal mode number, $n > 4$) are $m = 1$, making $\tilde{b}_{\phi,n}/\tilde{b}_{\theta,n} = na/R$. An empirical factor is used to obtain the total amplitude of the modes with toroidal mode number $n \leq 4$ (which are $m = 0$) from the measured poloidal component. The total rms fluctuation is then determined by adding the power in all resolved modes [$\tilde{b}_{rms} = (\sum \tilde{b}_n^2/2)^{1/2}$].

The total rms (over 5 ms) magnetic fluctuation is shown versus the Lundquist number in Fig. 6 for (a) low I_ϕ/N and (b) high I_ϕ/N . We find that the Lundquist number is not the unique dimensionless scaling parameter for the magnetic fluctuations in MST. At low I_ϕ/N (high relative density), the fluctuation amplitude scales with a power of S equal to -0.18 ± 0.01 . This scaling is in agreement with recent resistive MHD simulation results.^{14,21} However, at high I_ϕ/N , the fluctuations scale with S to the -0.07 ± 0.01 power, a weaker scaling. There is more scatter in the data at the highest values of S .

As a test of the sensitivity of the scaling relation $\tilde{b} \propto S^{-\alpha}$, to the measurement of Z_{eff} , and in order to compare our results to those of Hattori *et al.*²² we calculate the scaling exponent, α , assuming a constant $Z_{eff} = 2.0$. Figure 7 shows a somewhat stronger scaling for the magnetic fluctuations un-


 FIG. 7. The Lundquist number scaling of the magnetic fluctuations where $Z_{eff} = 2.0$ (constant) was assumed in calculating S .

 FIG. 8. A comparison of the Lundquist number scaling magnetic fluctuations in MST with the scaling obtained in OHTe. The Lundquist number was calculated by the same method as La Haye *et al.*

der this assumption ($S^{-0.28(\pm 0.02)}$) at low I_ϕ/N . This result is in good agreement with the scaling obtained on TPE-1RM15, where changes in Z_{eff} were not resolved and the Lundquist number was determined from previously measured density and temperature scaling with plasma current.

Two principal conclusions can be drawn from the scaling of the average magnetic fluctuations. First, the Lundquist number does *not* appear to be a unique dimensionless scaling parameter in MST. The observed scaling depends on relative density. This result suggests the need for a second dimensionless parameter to describe the fluctuation scaling. However, we point out that the range of scaling exponents obtained is narrow and small variations in the profiles (e.g., resistivity) that are not resolved by the global Lundquist number may explain some of the variation in the measured exponents. Second, the scaling is weaker than $S^{-1/2}$ seen in previous experiments⁶ and predicted by some MHD theories.^{16,17} This result is robust and cannot be explained by reasonable variation of the profiles.

LaHaye *et al.*⁶ reported the first measurements of the scaling of magnetic fluctuations with S in the RFP. They found $\tilde{b} \propto S^{-1/2}$ in the OHTe device. A comparison with the work of LaHaye *et al.* is obtained by calculating the scaling of fluctuations with the Lundquist number of Eq. (9), the “anomalous” Lundquist number. Figure 8 shows the MST data at low I_ϕ/N , and a representative region indicating where the OHTe data lies. Varying the anomalous Lundquist number, the MST fluctuations scale with an exponent of $-0.30 (\pm 0.02)$, significantly weaker than $S^{-0.51}$ seen in OHTe. However, the range of Lundquist numbers accessible in the two experiments do not overlap.

V. SCALING OF CONFINEMENT

A. Energy confinement time

To investigate the scaling of the energy confinement with the Lundquist number, we define a global energy confinement time as

$$\tau_E = \frac{9\bar{n}(T_{e0} + T_i)V}{8P_\Omega}, \quad (10)$$

where V is the plasma volume and $P_\Omega \approx I_\phi V_\phi$ is the Ohmic input power. Equation (10) makes use of an assumed para-

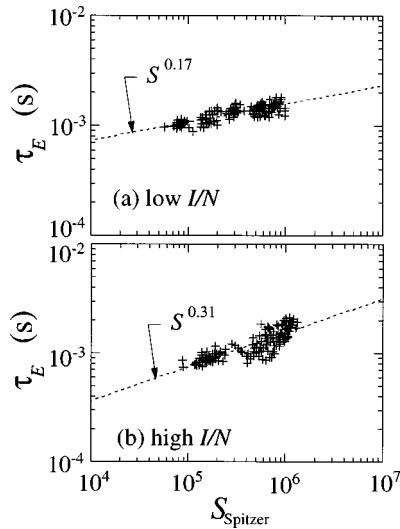


FIG. 9. The scaling of the energy confinement time with the Lundquist number.

bolic density profile [$n = n_0(1 - (r/a)^2)$] and a flat temperature profile, consistent with limited profile measurements in MST. At low I_ϕ/N the energy confinement time increases as $\tau_E \propto S^{0.17}$ (Fig. 9), whereas at high I_ϕ/N , the scaling is $\tau_E \propto S^{0.31}$. Since magnetic fluctuations are understood to be responsible for core transport in the RFP,^{23,24} the qualitative trends upward in Fig. 9 are expected; magnetic fluctuations are smaller at higher S , leading to higher τ_E . Quantitatively, the observation that confinement increases more rapidly with S at high I_ϕ/N is unexpected, since magnetic fluctuations scale more weakly with the Lundquist number for that case.

B. Stochastic transport scaling and implications for RFP reactor

Thermal diffusivity in the presence of a stochastic magnetic field is expected to obey the Rechester–Rosenbluth diffusivity equation,³⁶

$$\chi_{RR} \approx \left\langle \frac{\overline{B_r^2}}{B_0^2} \right\rangle v_{\text{the}} L, \quad (11)$$

where L is the parallel correlation length for the turbulence in the collisionless limit (~ 1 m in MST). Previous experiments in MST (at fixed control parameters) indicated that Eq. (11) holds with the electron thermal velocity replaced by the ion thermal velocity, and a theoretical argument has been made to explain the result.³⁷ The scaling of confinement with fluctuation amplitude and temperature predicted by Eq. (11) is tested here. A global experimental diffusivity is estimated by $\chi_{\text{expt}} = a^2/4\tau_E$, and the ratio of the Rechester–Rosenbluth diffusivity [Eq. (11)] to the experimental value is plotted versus the Lundquist number in Fig. 10. In the parameter regime most relevant for extrapolation toward reactor conditions, namely low I_ϕ/N , the stochastic transport model [Eq. (11)] predicts the observed confinement scaling; the ratio of χ_{RR} to χ_{expt} is relatively constant. The magnitude of the Rechester–Rosenbluth diffusivity is roughly a square root of the mass ratio (ion to electron) greater than the experimental

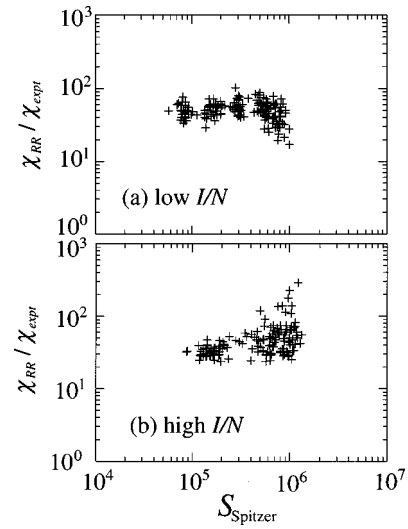


FIG. 10. A comparison of the experimental, global heat diffusivity, χ_{expt} , in MST with the expected value for transport in a stochastic magnetic field, χ_{RR} , versus the Lundquist number.

value, consistent with the ambipolar energy transport calculations of Terry *et al.*³⁷ for the RFP. At high I_ϕ/N the ratio rises weakly with S due to the stronger scaling of the confinement time in that regime.

A scaling relation for $n\tau_E$ can be derived for arbitrary power law scaling of magnetic fluctuations with Lundquist number, $\tilde{b} \propto S^{-\alpha}$, based on the stochastic field diffusivity. Take temperature, beta, minor radius, and plasma current to be free parameters. Then

$$n\tau_E \propto \beta^{1-\alpha} \cdot T^{4\alpha-3/2} \cdot a^{2\alpha-1} \cdot I_\phi^2, \quad (12)$$

where $\tau_E \propto a^2/(\tilde{b}^2 \sqrt{TL})$, $L \propto a$, $S \propto I_\phi T^{3/2}/\sqrt{n}$, and $\beta \propto a^2 n T / I_\phi^2$ have been used, and Z_{eff} is assumed constant. The most recent RFP reactor design study was TITAN ($a = 0.6$ m, $I_\phi = 18$ MA) (see Ref. 38 and references cited therein). The TITAN design point was extrapolated from the existing experimental database of the “best” confinement data from a number of RFP devices using an empirical fit to a theoretical scaling law.³⁸ In terms of the parameters used in Eq. (12), the scaling law employed was $n\tau_E \propto T^{1/2} \cdot a^0 \cdot I_\phi^2$ (independent of the minor radius), and approximately constant beta. If the magnetic fluctuations scale as $\tilde{b} \propto S^{-1/2}$ and β is held constant, then Eq. (12) recovers the scaling of DiMarco and Werley *et al.*³⁸ In a single device, e.g., MST, the DiMarco–Werley scaling law is not obeyed, partly due to the fact that experimental beta values fall with increasing plasma current.

Using Eq. (12) and benchmarking the coefficient of proportionality to present MST conditions, we can predict the exponent in the scaling relation for the magnetic fluctuations that is required to achieve fusion breakeven ($n\tau_E \approx 10^{20}$ s/m³ at $T = 10$ keV) at a given plasma current, minor radius, and β . Figure 11 shows the required exponent versus the plasma current for the TITAN size ($a = 0.6$ m) and a beta value of 25%. At the TITAN design current of 18 MA, the required exponent is about 0.4. The measured exponent at low I_ϕ/N ($\alpha \approx 1/5$) suggests more than 50 MA may be re-

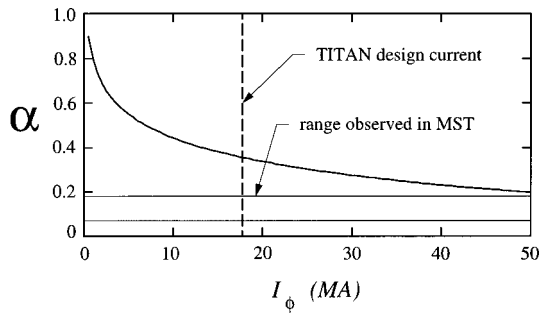


FIG. 11. The Lundquist number scaling exponent for magnetic fluctuations required to achieve the breakeven versus RFP plasma current at $\beta = 25\%$, $T = 10$ keV, and $a = 0.6$ m, parameters for the TITAN RFP reactor study.

quired. In addition, the TITAN design relied solely on Ohmic heating to reach the ignition at 25% beta. In MST, beta is seen to fall with increasing Lundquist number (Fig. 12) at constant I_ϕ/N without auxiliary heating. No auxiliary heating experiments have been performed on a RFP experiment, but experiments in tokamak plasmas show that auxiliary heating leads to confinement scaling relations quite different from those observed in Ohmic devices. Whether Eqs. (11) and (12) are relevant to auxiliary heated RFPs awaits determination by future experiments. If a scaling exponent of $\alpha \approx 1/5$ is assumed, consistent with the results in MST, then Eq. (12) becomes $n\tau_E \propto \beta^{4/5} \cdot T^{-7/10} \cdot a^{-3/5} \cdot I_\phi^2$. The somewhat counterintuitive dependence on minor radius and temperature arises because of the choice of independent parameters. For example, increasing the minor radius while holding the other parameters constant reduces the $n\tau_E$ product, partly because density must be reduced to hold β constant.

Fluctuation and confinement scaling in present (Ohmic) devices extrapolates pessimistically to reactor conditions. However, recent experiments in MST have demonstrated significant fluctuation reduction and consequent confinement improvement using current profile control.^{39,40} The experiments demonstrated a significant reduction of magnetic fluctua-

tions ($\sim 50\%$) associated with core resonant resistive tearing modes and simultaneous four- or fivefold improvement in energy and particle confinement. A RFP with current profile control could operate with much lower fluctuation levels and much better confinement than past and present devices, although it is not possible from experiments performed to date to assess the confinement scaling or the reactor attractiveness of a RFP with optimized current profile control. Electrostatic current injection,⁴¹ radio-frequency current drive in the lower hybrid range of frequencies⁴²⁻⁴⁴ and fast magnetosonic wave current drive⁴⁵ are being studied as possible steady-state current profile control techniques.

VI. SCALING OF SAWTOOTH FEATURES

A. Velocity fluctuations and Ohm's law

From Eq. (3) it is expected that the product of velocity fluctuations (normalized to the Alfvén velocity) and magnetic fluctuations (normalized to the mean field) should scale as $\tilde{b}\tilde{v} \propto S^{-1}$, if the single-fluid parallel Ohm's law is valid and if the relative phase between the two fluctuating fields is constant. Since magnetic fluctuations scale weaker than $S^{-1/2}$, velocity fluctuations should scale with a larger exponent (more negative) of S .

A fast Doppler spectrometer has been developed to measure toroidal flow velocity fluctuations of a core impurity species (C^{+4}).⁴⁶⁻⁴⁸ Impurity ion flow is expected to represent the majority ion (fluid) flow on the time scales of interest. Since flow velocity and magnetic field are the two vector fields of interest for the MHD model of plasma dynamics, the measurement of flow velocity as well as the magnetic field has the potential to provide much more detailed tests of MHD predictions than have been done in the past. In this paper we report on first time measurements of the scaling of velocity fluctuations in a hot, magnetized plasma.

During the S -scaling experiment the velocity fluctuations were resolved near the time of the sawtooth crash events when both magnetic and velocity fluctuations are largest. Away from the time of the crash, the C^{+4} emission intensity was too low to resolve the fluctuation amplitude. Figure 13 shows the (a) velocity fluctuation amplitude and (b) the magnetic fluctuation amplitude relative to the time of the sawtooth crash (averaged over ~ 30 sawtooth events) for one set of conditions at low I_ϕ/N . For the case shown, the magnetic fluctuation level reaches $\sim 4.5\%$ of the mean field. The rms velocity fluctuation reaches $\sim 3\%$ of v_A , where the Alfvén velocity was calculated using the surface poloidal magnetic field and the central chord-averaged density. The spectrometer collects light along a horizontal chord that averages over ~ 1.5 wavelengths for the dominant modes. The spatial average effectively attenuates the local fluctuation amplitude by a factor of order 5. The data shown in Fig. 13 have been multiplied by five to account for this effect, although there is substantial uncertainty in the correction factor at this time ($\sim 50\%$). Using the best estimate for the correction factor, the magnetic fluctuation amplitude is ~ 1.5 times the velocity fluctuation amplitude. This ratio is in rough agreement with predictions from MHD simulations

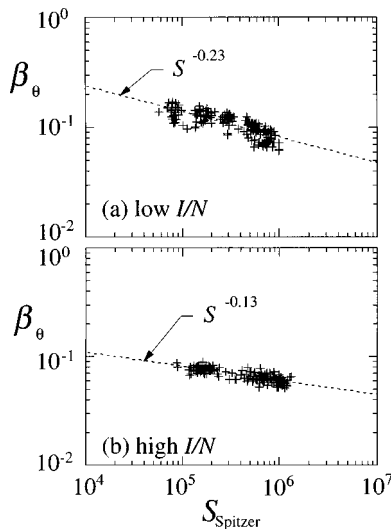


FIG. 12. Scaling of poloidal beta with the Lundquist number in MST.

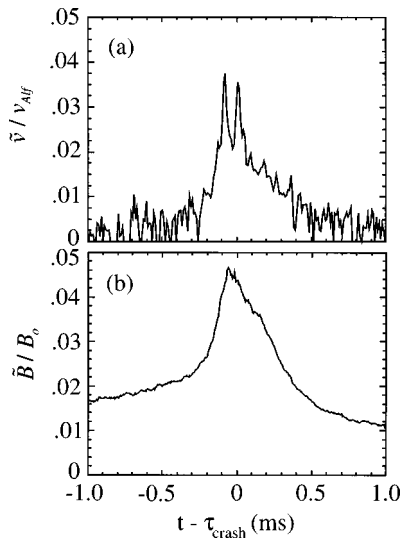


FIG. 13. (a) Velocity fluctuation amplitude (measured by Doppler spectroscopy) relative to the time of the sawtooth crash, and (b) magnetic fluctuation amplitude over the same time window. Signals are averaged over ~ 30 sawtooth events at low I_ϕ/N , and plasma current around 300 kA.

(after taking into account differences in the calculated Alfvén velocity).⁴⁹

Since the fluctuation amplitude was not resolved between sawtooth events, the scaling of the peak value of the velocity fluctuation near the sawtooth crash was examined. The rms fluctuation was calculated over a $100 \mu\text{s}$ interval around the time of the crash. The scaling of the peak velocity fluctuation is compared to the peak magnetic fluctuation amplitude in Fig. 14 for the low I_ϕ/N parameter space trajectory of Fig. 1. Velocity fluctuations fall off more rapidly with S than magnetic fluctuations ($\tilde{v}_{\text{peak}} \propto S^{-0.16}$, $\tilde{b}_{\text{peak}} \propto S^{-0.07}$), and the product of the fluctuation amplitudes scales weaker than the expected $\tilde{b}\tilde{v} \propto S^{-1}$. This measurement is not definitive since the average velocity fluctuation (over the sawtooth cycle) was not resolved, but it is suggestive that the relative phase between \tilde{v} and \tilde{b} is *not* constant with changes in S . Efforts are underway to resolve the scaling of the average velocity fluctuation as well as the relative phase between \tilde{v} and \tilde{b} .

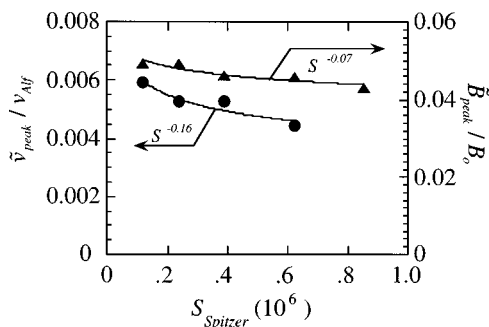


FIG. 14. Lundquist number scaling of the peak fluctuation amplitudes through the sawtooth cycle (at low I_ϕ/N).

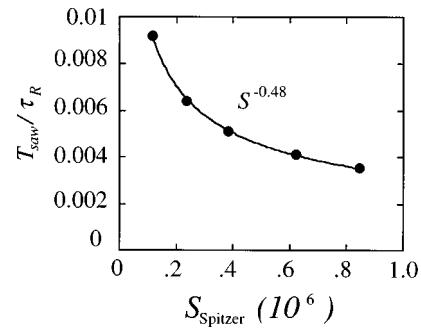


FIG. 15. Scaling of the normalized sawtooth period.

B. Sawtooth period

In the past, the RFP sawtooth oscillation was modeled as a slow resistive decay of the current profile, followed by a rapid reconnection event (crash) that reset the current profile.^{50,11} However, the resistivity profile that was required to model the decay phase of the oscillation was somewhat unphysical (or anomalous). We report an experimental measurement of the scaling of the sawtooth period that indicates a hybrid resistive-MHD character as opposed to a purely resistive character to the “decay phase.” The sawtooth period for the low I_ϕ/N scan was calculated and normalized to the resistive diffusion time (Fig. 15). Since the decay phase dominates the total sawtooth period, if the decay was purely resistive, the normalized period would be constant. The experiment shows the normalized period scaling as $\sim S^{-1/2}$, or that the absolute period scales as $T_{\text{saw}} \propto \sqrt{\tau_R \tau_A}$. The sawtooth period is governed by a hybrid time scale, not a purely resistive diffusion time. This result is in good agreement with the simulation results of Capello and Biskamp,¹⁴ who find $T_{\text{saw}} \propto \tau_R^{0.6} \tau_A^{0.4}$.

VII. DISCUSSION AND CONCLUSIONS

The results presented here extend the database of fluctuations scaling in the RFP to a higher Lundquist number and make use of a more complete determination of the resistivity than has been possible on previous experiments. Measurements of the scaling of the mean ion charge Z_{eff} in MST indicate that there is significant aluminum contamination at low current and low density. Impurity contamination contributes to enhanced classical resistivity and therefore to a reduction of the Lundquist number in that parameter regime.

The magnetic fluctuation amplitude was not found to be a unique function of Lundquist number, scaling with different exponents at high I_ϕ/N (-0.07) and low I_ϕ/N (-0.18). The range of scaling exponents obtained is narrow and excludes an important body of theoretical predictions that have been used to predict RFP reactor characteristics. Those theories that predict $\tilde{b} \propto S^{-1/2}$ are at odds with our measurements in MST. Our results suggest that another dimensionless parameter (other than the Lundquist number) may be important in the RFP, but we are hesitant to make this a definitive conclusion. The Lundquist number was de-

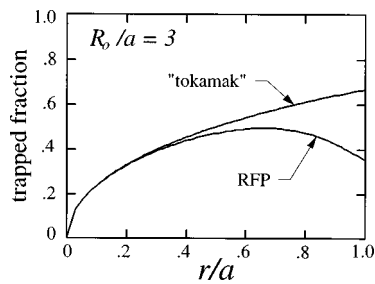


FIG. 16. The trapped particle fraction versus the minor radius for a typical toroidal equilibrium solution for a circular cross-section RFP at an aspect ratio of 3. The trapped fraction for a purely toroidal magnetic field at the same aspect ratio ("tokamak") is shown for comparison.

terminated from global measurements, and a modest profile variation may be responsible for some of the observed variation in the scaling exponent. We also point out that the work of Mattor¹⁹ predicts two scaling exponents of the fluctuations, $\tilde{b} \propto S^0$ for discrete dynamo fluctuations (e.g., sawteeth) and $\tilde{b} \propto S^{-1/4}$ for continuous dynamo fluctuations. This fairly narrow range of predicted exponents ($0 < \alpha < 1/4$) bracket the experimentally observed scaling exponents ($0.07 < \alpha < 0.18$). Probe measurements of the dynamo electric field in the outer region of the plasma demonstrate the existence of both a continuous and a discrete component.⁸ Those measurements could only be carried out in relatively high-density, low plasma current conditions, so it was not possible to assess the extent to which the discrete dynamo component may dominate at lower density.

At low I_ϕ/N the stochastic diffusion model is in good agreement with the experimental scaling, providing a physical basis for a confinement scaling law for Ohmic RFPs [Eq. (12)]: $n\tau_E \propto \beta^{4/5} \cdot T^{-7/10} \cdot a^{-3/5} \cdot I_\phi^2$. The pessimistic extrapolation of this scaling to reactor conditions suggests that an auxiliary fluctuation suppression measure such as current profile control or active feedback will be a necessary element of any RFP reactor design.

The scaling of MHD velocity fluctuations has been examined for the first time by measuring the peak fluctuation level during the sawtooth oscillation. The velocity fluctuations scale with a larger exponent of S than the peak magnetic fluctuations, but not large enough to satisfy the simplest scaling expectations based on the single fluid parallel Ohm's law. The period of the RFP sawtooth oscillation is found to be determined by a hybrid time scale, $T_{\text{saw}} \propto \sqrt{\tau_R \tau_A}$, consistent with simulation results, but at odds with previous experiments that modeled the sawtooth rise as a purely resistive diffusion process. Future work will examine the scaling of the average velocity fluctuation as well as the relative phase between the velocity and magnetic fluctuations.

ACKNOWLEDGMENTS

The authors would like to thank Nathan Mattor and Carl Sovinec for valuable conversations that contributed to this work.

This work is supported by the U.S. Department of Energy, Grant No. DE-FG02-96ER54345.

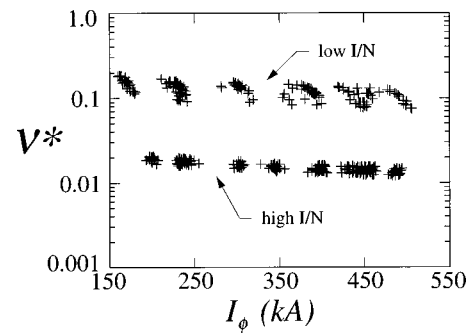


FIG. 17. Electron collision frequency normalized to the trapped particle bounce frequency for the S scaling database in MST.

APPENDIX: TRAPPED PARTICLES IN THE RFP

Trapped particle fractions were investigated using a toroidal equilibrium code written to provide equilibria for the Madison Symmetric Torus (MST), a circular poloidal cross section RFP with aspect ratio $R_0/a = 3$.²⁵ Equilibrium is provided passively in MST by the 5 cm thick close-fitting aluminum shell ($\tau_{\text{shell}} > \tau_{\text{pulse}}$). The code solves the Grad-Shafranov partial differential equation,⁵¹ including a physically reasonable pressure profile ($\beta_p \sim 7\%$). The normalized parallel current profile [which determines $F(\psi)$] is prescribed to be flat out to a critical flux surface, outside of which it falls to zero at the boundary [note: a constant normalized current out to the surface would be a minimum magnetic energy (Taylor) state⁵²]. The code is therefore a toroidal adaptation of the so-called modified Bessel function model (MBFM),⁵³ the profiles of which are accurately reproduced by the present code at a large aspect ratio. The surface of the conducting shell is assumed to be a constant flux contour (the shell time is ~ 300 ms compared to a typical discharge duration of 60 ms).

Assuming the velocity space distribution to be isotropic, the results for a typical set of MST parameters are shown in Fig. 16. The trapped particle fraction is plotted versus the normalized minor radius. Also shown is the trapped particle fraction for a "tokamak" of the same aspect ratio, i.e., $B = B_0 R_0/R$. The trapped particle fraction in the RFP is very similar to the fraction trapped in a dominantly toroidal (\sim tokamak) field out to nearly the half-radius. Near the surface of the RFP, the trapped fraction is smaller than for the tokamak and is sensitive to the chosen current profile. In fact, for a very peaked current profile, the RFP can have a trapped particle population near the surface that is trapped in the inboard side of the device; i.e., the mirror ratio can reverse sign with a radius. For the case shown in Fig. 16, the cross section integrated trapped particle fraction is 38% for the RFP and 42% for the tokamak.

The presence of a significant trapped particle population in the RFP does not lead to large neoclassical effects. The ion banana orbit widths are comparable to the ion Larmor radii because the poloidal field magnitude is comparable to the toroidal field magnitude. Therefore, neoclassical diffusion coefficients are comparable to classical diffusion coefficients, bootstrap current is small, etc. The presence of trapped particles is deleterious to the use of low-frequency

(Alfvén wave) current drive in the RFP.⁵⁴ In the collisionless regime, the trapped particle fraction does not participate in carrying current and therefore enhances the classical, Spitzer resistivity. The appropriate measure of collisionality is the ratio of the collision frequency to the bounce time for a trapped particle, $\nu^* \equiv \nu_e / \nu_b$. In the RFP, the bounce frequency is of order $\nu_b \approx v_{th} / 2\pi a$. Values for ν^* are shown in Fig. 17 for the *S*-scaling database in MST. All shots in the database are in the collisionless or banana regime.

¹A. Sykes and J. A. Wesson, in *Proceedings of the 8th European Conference on Plasma Physics and Controlled Fusion*, Prague (European Physical Society, Petit-Lancy, Switzerland 1977), Vol. I, p. 80.
²A. Y. Aydemir and D. C. Barnes, *Phys. Rev. Lett.* **52**, 930 (1984).
³D. D. Schnack, E. J. Caramana, and R. A. Nebel, *Phys. Fluids* **28**, 321 (1985).
⁴K. Kusano and T. Sato, *Nucl. Fusion* **27**, 821 (1987).
⁵I. H. Hutchinson, M. Malacarne, P. Noonan, and D. Brotherton-Ratcliffe, *Nucl. Fusion* **24**, 59 (1984).
⁶R. J. La Haye, T. N. Carlstrom, R. R. Goforth, G. L. Jackson, M. J. Schaffer, T. Tamano, and P. L. Taylor, *Phys. Fluids* **27**, 2576 (1984).
⁷D. Brotherton-Ratcliffe, C. G. Gimblett, and I. H. Hutchinson, *Plasma Phys. Controlled Fusion* **29**, 161 (1987).
⁸H. Ji, A. F. Almagri, S. C. Prager, and J. S. Sarff, *Phys. Rev. Lett.* **73**, 668 (1994).
⁹R. G. Watt and R. A. Nebel, *Phys. Fluids* **26**, 1168 (1983).
¹⁰V. Antoni and S. Ortolani, *Phys. Fluids* **30**, 1489 (1987).
¹¹S. Hokin, A. Almagri, S. Assadi, J. Beckstead, G. Chartas, N. Crocker, M. Cudzinovic, D. Den Hartog, R. Dexter, D. Holly, S. Prager, T. Rempel, J. Sarff, E. Scime, W. Shen, C. Spragins, C. Sprott, G. Starr, M. Stoneking, C. Watts, and R. Nebel, *Phys. Fluids B* **3**, 2241 (1991).
¹²K. Kusano and T. Sato, *Nucl. Fusion* **30**, 2075 (1990).
¹³Y. L. Ho and G. G. Craddock, *Phys. Fluids B* **3**, 721 (1991).
¹⁴S. Capello and D. Biskamp, *Nucl. Fusion* **36**, 571 (1996).
¹⁵S. Assadi, S. C. Prager, and K. L. Sidikman, *Phys. Rev. Lett.* **69**, 281 (1992).
¹⁶C. A. Bunting, C. W. Gower, K. Ogawa, D. C. Robinson, and M. R. C. Watts, *Ref. 1*, p. 79.
¹⁷J. W. Connor and J. B. Taylor, *Phys. Fluids* **27**, 2676 (1984).
¹⁸Z. G. An, P. H. Diamond, R. D. Hazeltine, J. N. Leboeuf, M. N. Rosenbluth, R. D. Sydora, T. Tajima, B. A. Carreras, L. Garcia, T. C. Hender, H. R. Hicks, J. A. Holmes, V. E. Lynch, and H. R. Strauss, *Plasma Physics and Controlled Nuclear Fusion Research 1984*, Proceedings of the 10th International Conference (International Atomic Energy Agency, Vienna, 1985), Vol. II, p. 231.
¹⁹N. Mattor, *Phys. Plasmas* **3**, 1578 (1996).
²⁰H. R. Strauss, *Phys. Fluids* **29**, 3008 (1986).
²¹C. R. Sovinec, Ph.D. thesis, University of Wisconsin—Madison 1995, p. 91.
²²K. Hattori, Y. Hirano, T. Shimada, Y. Yagi, Y. Maejima, I. Hirota, and K. Ogawa, *Phys. Fluids B* **3**, 3111 (1991).
²³M. R. Stoneking, S. A. Hokin, S. C. Prager, G. Fiksel, H. Ji, and D. J. Den Hartog, *Phys. Rev. Lett.* **73**, 549 (1994).

²⁴G. Fiksel, S. C. Prager, W. Shen, and M. Stoneking, *Phys. Rev. Lett.* **72**, 1028 (1994).
²⁵R. N. Dexter, D. W. Kerst, T. W. Lovell, S. C. Prager, and J. C. Sprott, *Fusion Technol.* **19**, 131 (1991).
²⁶S. Ortolani and G. Rostagni, *Nucl. Instrum. Methods Phys. Res.* **207**, 35 (1983).
²⁷L. Spitzer, Jr. and R. Harm, *Phys. Rev.* **89**, 977 (1953).
²⁸I. H. Hutchinson, *Principles of Plasma Diagnostics*, (Cambridge University Press, New York 1987), pp. 18–20.
²⁹S. P. Hirshman and D. J. Sigmar, *Nucl. Fusion* **21**, 1079 (1981).
³⁰K. F. Schoenberg, R. W. Moses, and R. L. Hagenson, *Phys. Fluids* **27**, 1671 (1984).
³¹T. R. Jarboe and B. Alper, *Phys. Fluids* **30**, 1177 (1987).
³²H. Y. W. Tsui, *Nucl. Fusion* **28**, 1543 (1988).
³³J. C. Sprott, *Phys. Fluids* **31**, 2266 (1988).
³⁴D. J. Den Hartog and M. Cekic, *Meas. Sci. Technol.* **5**, 1115 (1994).
³⁵S. Hokin, A. Almagri, M. Cekic, B. Chapman, N. Crocker, D. J. Den Hartog, G. Fiksel, J. Henry, H. Ji, S. Prager, J. Sarff, E. Scime, W. Shen, M. Stoneking, and C. Watts, *J. Fusion Energy* **12**, 281 (1993).
³⁶A. B. Rechester and M. N. Rosenbluth, *Phys. Rev. Lett.* **40**, 38 (1978).
³⁷P. W. Terry, G. Fiksel, H. Ji, A. F. Almagri, M. Cekic, D. J. Den Hartog, P. H. Diamond, S. C. Prager, J. S. Sarff, W. Shen, M. Stoneking, and A. S. Ware, *Phys. Plasmas* **3**, 1999 (1996).
³⁸K. A. Werley, J. N. DiMarco, R. A. Krakowski, and C. G. Bathke, *Nucl. Fusion* **36**, 629 (1996).
³⁹J. S. Sarff, N. E. Lanier, S. C. Prager, and M. R. Stoneking, *Phys. Rev. Lett.* **78**, 62 (1997).
⁴⁰M. R. Stoneking, N. E. Lanier, S. C. Prager, J. S. Sarff, and D. Sinitzyn, *Phys. Plasmas* **4**, 1632 (1997).
⁴¹D. Craig, A. F. Almagri, J. K. Anderson, J. T. Chapman, C.-S. Chiang, N. A. Crocker, D. J. Den Hartog, G. Fiksel, S. C. Prager, J. S. Sarff, and M. R. Stoneking, *Phys. Rev. Lett.* **79**, 1865 (1997).
⁴²E. Uchimoto, M. Cekic, R. W. Harvey, C. Litwin, S. C. Prager, J. S. Sarff, and C. R. Sovinec, *Phys. Plasmas* **1**, 3517 (1994).
⁴³S. Hokin, J. S. Sarff, C. R. Sovinec, and E. Uchimoto, *Nucl. Fusion* **34**, 1447 (1994).
⁴⁴R. A. Dziubek, R. W. Harvey, S. A. Hokin, and E. Uchimoto, *Nucl. Fusion* **36**, 453 (1996).
⁴⁵S. Shiina, Y. Kondoh, and H. Ishii, *Nucl. Fusion* **34**, 1473 (1994).
⁴⁶D. J. Den Hartog and R. J. Fonck, *Rev. Sci. Instrum.* **65**, 3238 (1994).
⁴⁷D. J. Den Hartog, A. F. Almagri, J. T. Chapman, H. Ji, S. C. Prager, J. S. Sarff, R. J. Fonck, and C. C. Hegna, *Phys. Plasmas* **2**, 2281 (1995).
⁴⁸J. T. Chapman and D. J. Den Hartog, *Rev. Sci. Instrum.* **68**, 285 (1997).
⁴⁹Y. L. Ho, Ph.D. thesis, University of Wisconsin—Madison, 1988, p. 71.
⁵⁰K. A. Werley, R. A. Nebel, and G. A. Wurden, *Phys. Fluids* **28**, 1450 (1985).
⁵¹See, for example, J. P. Freidberg, *Ideal Magnetohydrodynamics* (Plenum Press, New York, 1987), Chap. 6.
⁵²J. B. Taylor, *Phys. Rev. Lett.* **33**, 1139 (1974).
⁵³K. F. Schoenberg, R. F. Gribble, and J. A. Phillips, *Nucl. Fusion* **22**, 1433 (1982).
⁵⁴D. A. Ehst and C. F. Karney, *Nucl. Fusion* **31**, 1933 (1991).